MnO$_2$-ZnO Hexagonal Nanomaterials: Characterization and High Performance Humidity Sensing Application

Vikas Kumar Verma[1*], Narendra Kumar Pandey[2]

[1,2]Sensors and Materials Research Laboratory, Department of Physics, University of Lucknow, Lucknow, India

Corresponding Author Email: vikasverma37@gmail.com

Abstract---MnO$_2$ doped nanostructured zinc oxide was synthesized by solid state reaction route. The prepared material was characterized by X-ray diffraction, scanning electron microscope and UV-Vis absorption spectroscopy. The doping of MnO$_2$ in ZnÒ enhanced the crystallization and decreased the crystallite size. Surface morphology of the sensing material showed that the hexagonal shaped particles were uniformly distributed in zinc oxide that left large number of pores. These pores acted as humidity adsorption sites. With increase in the concentration of MnO$_2$, the pores also increased. The optical band gap of pure ZnO was 4.05 eV. The value of band gap decreased with increase in the MnO$_2$ doping concentration. The average sensitivity of undoped zinc oxide was 3400 KΩ/%RH. The sensitivity of the sensing element increased with increase in the doping concentration. Sensitivity of MnO$_2$ doped ZnO composite is more than four times the sensitivity of pure zinc oxide at annealing temperature 600°C.

Keywords---Humidity Sensor; Zinc oxide; X-ray diffraction; Scanning electron microscopy; UV-Vis Spectroscopy.

I. INTRODUCTION

Humidity plays an important role in human life. Its tremendous importance is due to the fact that its vapour consists of highly reactive dipolar molecules which get condensed on or evaporate from surface even with slight variation in temperature of the environment. It, therefore, becomes necessary to measure and control the humidity. The humidity is one of the most frequently measured quantities and its measurement is complex and an old problem too [1-2]. Humidity sensors convert the amount of water (H$_2$O) vapour into a measurable parameter. Humidity sensors based on different working principles have been developed and utilized in various applications [3–4]. Surface morphology has an important role in sensing properties. Researchers are developing cutting edge humidity sensors that show superb sensitivity, low hysteresis, and other amazing properties. Scientists are focusing more and more on impedance or resistive type humidity sensors due to low cost and better performance. The nano-grained ceramic materials provide opportunities for enhancing the performance of sensors because of their high surface to volume ratio. To enhance the sensing properties, therefore, it is essential to manipulate and control surface morphology so that high surface to volume ratio is available for effective sensing. To enhance sensing efficiency, some additives are used that play catalytic role. In the past few decades, metal oxide ceramic materials have attracted much attention of researchers due to their significant applications in microelectronic circuits, fuel cells, sensors, catalysts, optoelectronic devices and coatings for the passivation of surfaces with rust [5-11].

Zinc oxide (ZnO) is a versatile semiconductor with direct band gap of gap of ~3.37 eV and a large exciting binding energy of ~60 meV [12-13] at room temperature (RT). For photonic crystals ZnO is a promising candidate as functional components, gas sensors [14-15], light emitting diodes , solar cells, varistors and photo electrochemical cells [16-20]. ZnO nanomaterials has been synthesized with various structures and properties viz, nanoparticles, nanorods, nanocombs, nanowires, and tetrapod nanostructures [21-25]. Doping of selective element into ZnO is the primary method for manipulating and controlling its properties such as band gap or electrical conductivity, carrier concentration, etc. Studies have focused on the doping of transition metals Mn, Ni, Fe, Co and Cr into ZnO due to the potential applications in spintronics [26]. ZnO materials are believed to be non-toxic, bio-safe and biocompatible [27]. Doped and undoped ZnO nanostructures have the possibility of being applied for nano devices to detect gas and humidity because the response to different gases is related to a great extent to

the surface state and morphology of the material. ZnO does not need costly noble metal catalyst to perform as a good sensor. ZnO has also good temperature dependent surface morphology [28]. It shows an n-type semiconducting nature. Humidity sensor-elements based on ZnO have been fabricated in various forms, including single crystals, sintered pellets, thick films and thin films. ZnO nanomaterial-based elements show various useful properties and applications as humidity sensors [29-32]. It has fascinated much attention as humidity sensor because of its chemical sensitivity to volatile and radical gases, high chemical stability, easy doping, non-toxicity, and low cost [33-35]. ZnO is available in various morphologies [36-37]. Investigations were also carried out by Jeseentharani et al. for analysing humidity sensing properties of the composites prepared by mixing 1:1 mole ratio of CuO-ZnO, CuO-NiO, and NiO-ZnO compound. The samples were sintered at 800°C for 5 h and then subjected to resistance measurements as function of relative humidity (RH) in the range of 5%–98% RH. It was noticed that CuO-NiO compound possessed the best humidity sensitivity. The response and recovery times of the CuO-NiO composites were 80 and 650 s, respectively [38]. Kutteyet al. have reported the varistor properties of polycrystalline ZnO:Cu [39]. Yawale et al. doped semiconducting materials SnO_2 and ZnO with TiO_2 and Al_2O_3 and screen printed them in the form of a film. DC-electrical resistance of the films were measured in the presence of humidity. They found SnO_2-$5Al_2O_3$ and ZnO-$5Al_2O_3$ to be good sensing materials for humidity. Rutile and hexagonal structures of SnO_2, ZnO and Al_2O_3 and their nanometer grain sizes were found to be responsible for formation of nanometer sized pores, which ultimately adsorbed water. The adsorption of water (physisorbed water) on a hydroxylated surface caused electron injection [40]. Li et al. investigated the complex impedance spectra of the thin-film humidity sensors prepared using in situ synthesized inorganic/organic nanocomposites of sodium polystyrenesulfonate (NaPSS) and ZnO. The logarithm of the resistance of sensor based on composite film changed linearly by four orders of magnitude over the humidity range (11%–97% RH) [41]. Humidity sensors are also developed using capacitive technique. In this case the dielectric constant value of the thin film changes due to the change in the humidity level and in this way the relative humidity change is detected. The materials that are commonly used in the development of humidity-sensitive dielectrics are polyimide films. These materials provide high sensitivity, linear response, low response time, and low power consumption [42-45]. The performance of humidity sensing properties of the MnO_2-ZnO sensors compared with some other works in Table 1.The hysteresis and aging in all cases [52-54] were within ±2%. Sensitivity of humidity sensor is defined as the change in resistance (ΔR) of sensing element per unit change in RH (Δ% RH).

$$Sensitivity = (\Delta R)/(\Delta\%RH) \qquad\qquad (1)$$

The present work shows very high sensitivity results as compared to many reported works. Sensitivity of MnO_2-ZnO composite is more than six times the sensitivity of Ag-WO_3 nanomaterial and nearly four times Cu_2O-ZnO sensor, more than 1.5 times WO_3-SnO_2 sensor.

Table 1. Humidity sensing properties of the MnO_2-ZnO sensor compared with previous works.

Sensing Material	Sensor fabrication Method	Measurement range	Sensitivity	Reference
NiO-SnO_2	Electro spinning Technique	0-100%RH	3.25 KΩ/%RH	[46]
Sb-SnO_2	Vapour Liquid Solid Method	22-44%RH	100.454KΩ/%RH	[47]
$Bi_6S_2O_{15}$	Suspension Dripping	11-95%RH	118.929 KΩ/%RH	[48]
Black Phosphorus	Spin Coating	10-90%RH	124.975KΩ/%RH	[49]
SnO_2	Microwave Irradiation	5-95%RH	149.89 Ω/%RH	[50]
SnS_2-TiO_2	Layer-by-layer Self-Assembly	11-97%RH	442 KΩ/%RH	[51]
Ag-WO_3	Solid State Reaction	10-95%RH	2140 KΩ/%RH	[52]
Cu_2O-ZnO	Solid State Reaction	10-95%RH	4780 KΩ/%RH	[53]
WO_3-SnO_2	Solid State Reaction	10-95%RH	8790 KΩ/%RH	[54]
MnO_2-ZnO	Solid State Reaction	10-95%RH	13610 KΩ/%RH	**Present Work**

II. EXPERIMENTAL PROCEDURE

2.1 Synthesis of ZnO-MnO_2 Composite Pellets

The starting material was ZnO (Loba Chemie 98.0%). For binding the material 5% by weight of ethyl cellulose (LobaChemie) was used. The mixture was grinded for 3 hoursto homogeneity, and smaller crystalline size. The fine and grained powder of sample was pelletized with the help of hydraulic press machine (M.B. Instruments, Delhi, India) under an uniaxial pressure of 4 M Pa at room temperature. The dimensions of pellets were identical having 12 mm diameter and thickness 3 mm. The

pellets, then, were sintered for good nucleation and growth of the grains which were required for the sensing. This made surface to volume ratio higher. Sensing elements with 0%, 0.2%, 0.4%, 0.6%, 0.8% and 1.0% of MnO_2 in ZnO are labelled as Z_1, Z_2, Z_3, Z_4, Z_5 and Z_6, respectively.

2.2 Humidity Sensing Measurements

For the relative humidity (RH) sensing a special humidity chamber was designed which consisted of Cu-pellet-Cu electrode system well connected to the protruding electrodes of multimeter. In order to evaluate the sensing behaviour, the pellet was placed between the two copper electrodes. Humidity chamber used in this investigation consisted of a steel container having an air tight and movable glass lid to cover it. Two glass bowls were kept inside it one by one; one contained saturated aqueous solution of KOH to dehumidify the chamber up to 10%RH and other contained saturated aqueous solution of K_2SO_4 to humidify the chamber up to 95%. Pellet was put within this system and sensing measurements were performed. Variations in humidity inside the chamber were recorded by a standard hygrometer associated with a thermometer (Huger, Germany) and corresponding variation in electrical resistance was measured by multi-meter (Model VC9808). The least count of hygrometer used here was ±1%RH.

2.3 UV-Vis Spectroscopy

UV–Vis absorption spectrophotometer (Model− V670, Jasco) in UV and visible ranges from 200-800 nm was used for optical measurements.The typical UV-visible spectra of MnO_2 doped zinc oxide are shown in the Figure 1.The spectrum of each composition shows a sharp intense absorption band at energies close to the optical band gap that manifests itself as an absorption edge (as shown in Figure 1a). The optical band gap is calculated by extrapolation of linear plot (Tauc plot) between absorption coefficient (α) and photon energy as described in given equation [55]:

$$\alpha(h\nu) = (h\nu - E_g)^{1/2} \tag{2}$$

here, E is the photon energy and E_g is the optical band gap energy of the material. This equation shows a linear dependence of $\alpha^2(h\nu)$ on photon energy (E). Figure 1(b) show the Tauc plots of α^2 ($h\nu$) versus photon energy ($h\nu$). The optical band gap of undoped zinc oxide was found 4.05 eV. The value of optical band gap decreased with increase in MnO_2 concentration. The decrease in the value of band gap in the present study shows the red shift with increase of MnO_2 concentration. Value of optical band gap are 4.05, 4.05, 4.02, 3.95, 3.90 and 3.85 for 0.0%, 0.2%, 0.4%, 0.6%, 0.8% and 1.0% doping of MnO_2 in ZnO, respectively.

2.4 Scanning Electron Microscopy

The surface morphology of well-polished samples were examined using scanning electron microscope (model LEO 430 Cambridge Instruments Ltd., U. K.). Annealing process reduces the residual stress on the surface of the materials. The grains become ordered in a specific manner leaving some more spaces among them. Due to the annealing process, the size of pores increases. The re-crystallization process during the annealing has two stages, in the beginning; the re-crystallization is dominated by random orientation of the grains followed by a second process in which once again the crystallites tend to orient in a particular direction. Due to their particular orientation/alignment, the surface morphology changes. The typical microstructure of undoped and 0.2, 0.4, 0.6, 0.8 and 1.0 weight% MnO_2 doped zinc oxide and annealed at temperatures 600˚C are shown in Figures 2 (a-f). Figure 2(a) reveals that nanoparticles of ZnO agglomerate with one another leaving some spaces as pores. These pores serve as humidity adsorption sites and humidity sensitivity of the sensor depends on the size of these pores. Most of the particles are hexagonal in shape leaving more space as pores, giving effective surface area due to nano-sized surface morphology. The microstructure of 0.2 weight% MnO_2 doped zinc oxide shows almost similar pattern microstructure as that of pure ZnO, only a little bit difference of degree of crystallization and pores size [as shown in Figure 2(b)]. As the doping % of MnO_2 was increased from 0.2 weight% to 0.4 weight%, the agglomeration of MnO_2 becomes visible as shown in SEM image Figure 2(c). This agglomeration may increase the conductivity which decreases resistance more rapidly with adsorption of moisture. With further increase of doping concentration from 0.4 weight% to 0.6 weight%, the crystallization of zinc oxide was found to be higher as compared to lower doping concentration of MnO_2. This increase in size and number of pores are helpful for sensing the humidity (Figure 2d). The shape of crystallite also changes from hexagonal to rectangular shaped crystallites. As shown in Figure 2(e) at 0.8 weight% doping of MnO_2 in zinc oxide, the shape of crystallites becomes mixed of spherical and rectangular, the higher degree of pores is may be attributed in the sample to the distribution in grain size. The better crystallization is observed at this doping concentration of 1.0 weight% of MnO_2, as reflected in Figure 2 (f). The grain size for a fixed percentage of doping decreased when annealing temperature was increased. When annealing temperature was increased from 500°C to 600°C the grain size for 0.2% doping from 268 nm to 218 nm, for 0.4% doping from 251 nm to 208 nm, for 0.6% doping from 228 nm to 198 nm and for 1.0% doping from 223 nm to 192 nm. However, no definite trend was observed in the grain size measurement from SEM when doping percentage was increased for fixed annealing temperature.

2.5 X-ray Diffraction

The well prepared undoped and doped zinc oxide were characterized by X-ray powder diffraction (XRD) employing Rigaku Miniflex-II X-ray diffractometer using Cu-K$_{\alpha 1}$ radiation having wavelength $\lambda = 1.5406$ Å. The intensity was recorded over 2θ range 20–80° for phase identification. The average crystallite size of powdered samples were calculated by Debye-Scherer equation. The surface morphology of prepared samples were polished with 100, 600, 1000 mesh SiC powder as well as 1/0, 2/0, 3/0 and 4/0 grades sand paper, etched with 30% HNO_3 + 20% HF solution and coated with silver-palladium (Portion Sc-7640 Sputter). The typical X-ray diffraction patterns of undoped and 0.2, 0.4, 0.6, 0.8, 1.0 weight% MnO_2 doped zinc oxide are shown in the Figure 3. These patterns are well matched with standard JCPDS file No. 79-2205. The results clearly indicate that the prominent peaks in the patterns correspond to hexagonal wurzite structure of zinc oxide [56].

Crystallite size was calculated using the broadening of XRD peaks by the Debye-Scherer formula which is as follows**:**

$$D = \frac{K\lambda}{\beta \, Cos\theta} \tag{3}$$

Where β is the full width at half maximum (FWHM) of the peak, λ is X-ray wavelength, θ is the Bragg angle and K = 0.94, a dimensionless constant. The crystallite sizes were found to be 49.7, 46.5, 43.3, 40.9, 35.0 and 31.7 nm for 0.0, 0.2, 0.4, 0.6, 0.8 and 1.0 weight% MnO_2 doped zinc oxide, respectively. The crystallite size decreased with increasing the concentration of MnO_2. The sharp intense peaks of ZnO confirms the good crystalline nature of ZnO and the diffraction peaks can be indexed to a hexagonal wurtzite structured ZnO; for the MnO_2 doped ZnO the centres of all diffraction peaks have a slight shift compared to undoped sample.

III. RESULTS AND DISCUSSION

The change in the value of resistance has been recorded with change in the %RH for different annealing temperatures. With change in %RH the fall in the value of resistance is very sharp; ranging from 200-300 MΩ to 0-10 MΩ over 10 to 99% RH. Hence, a graph between the logarithmic resistance value and %RH has been plotted. Figure 4 shows graphs for the pure ZnO, 0.4% MnO_2 doped ZnO and 1.0% MnO_2 doped ZnO, for the annealing temperature of 600˚C. Figure 4 also shows trend line of graphs for the 0.4% and 1.0% MnO_2 doped ZnO. Both of these trend lines match polynomial of degree 3 as depicted in the figure itself.

The average sensitivity of the MnO_2 doped ZnO sensor increases with increase in the annealing temperature as well as the doping concentration of MnO_2. When annealing temperature is increased from 300˚C to 600˚C for pure ZnO the sensitivity increased from 2.1 MΩ/%RH To 3.4 MΩ/%RH. Similarly, when the annealing temperature is increased from 300˚C to 600˚C for 1.0% doped sample the sensitivity increased from 10.41 MΩ/%RH to 13.61 MΩ/%RH. As the annealing temperature is increased the larger pores are created on the surface of sensing pellets. When the doping of MnO_2 is increased better crystallization of zinc oxide takes place which creates more pores on the sensing pellet surface. As pore size increases on annealing the pellet adsorbs more moisture from the air which causes change in the resistance of the sensing material. The change in resistance of samples depends upon the active surface sites for the adsorption of moisture. If more sites of adsorption are found more will be the sensitivity of the sensor.

Sensitivity increases with increase in the percentage of the doping. With increase in the concentration of MnO_2 the XRD peaks slightly shifted to higher Bragg angles compared to those for the pure ZnO sample. The diffraction angle for the ZnO peak [101] at 2-theta value of 35.1097 shifted to 35.2528 for 0.4 weight % MnO_2 doped ZnO and to 35.2844 for 1.0 weight % MnO_2 doped ZnO. Such changes are indeed expected if some of the Mn ions replace Zn ions in the lattice, as the Mn ions have smaller ionic radii [Mn^{4+} (0·056 nm) and Mn^{3+} (0·062 nm)] than Zn ions (0.74Å). The shift indicates decrease of lattice parameters [57]. Some mechanisms were proposed to explain the surface conductivity change in the presence of water vapour [58-60]. The surface first experiences the chemisorption of monolayer water with proton transfer among hydronium (H_3O+). Here, the electrical response depends on the number of water molecules adsorbed on the surface. The chemisorption is followed by physisorption of multilayer water with increase in humidity. Here, H_3O^+ appears in the physisorbed water and serves as a charge carrier. H^+ ions can move freely in the physisorbed water according to Grotthuss's chain reaction [61-62]. At high humidity, electrolytic conduction replaces protonic conduction. Doping Mn ions into ZnO leads to higher charge density on the surface. In this case, a strong electric field is induced around the surface of Mn-doped ZnO. This strong electric field augments ionization of water molecules and further affects the deeper physisorbed water. As the doping % increases more Mn ions get incorporated into ZnO lattice. This leads to higher charge density in the vicinity resulting in creation of a stronger electric field near the surface. When water vapours interact with the surface this high field causes ionization of water molecules

leading to high conductivity. Thus the sensitivity increases with increase in concentration of MnO_2 in ZnO [63]. Figure 5 shows graph for the change in the sensitivity of the samples both for the increase in the annealing temperature and the change in percentage of the MnO_2 in ZnO. A linear trend line is the best match for the sensitivity versus % RH graphs as shown in the figure for each annealing temperature. For annealing temperature 300˚C the sensitivity increases from 2.1 MΩ/%RH to 10.41 MΩ/%RH when the doping is increased from 0.0% to 1.0%. For annealing temperature 600˚C the sensitivity increases from 3.4 MΩ/%RH to 13.61 MΩ/%RH when the doping is increased from 0.0% to 1.0%.

Hysteresis in metal oxides is attributed to the initial chemisorptions on the surface of the sensing elements. This chemisorbed layer is generally irreversible and can't be easily removed by decreasing %RH. This layer can be desorbed using thermal means only. The physisorption is reversible and the layer can be easily desorbed. Hence, in the decreasing cycle of % RH, the initially adsorbed water is not removed completely leading to hysteresis. Metal oxides and binary systems of metal oxides show deviation in their behaviour in the decreasing cycle of %RH from those in increasing cycle of %RH. Minimization of this hysteresis behaviour is a condition a priori for sensor applications. To determine the hysteresis effect in the sensing elements, the humidity in the chamber has been increased from 10% RH to 99% RH and then cycled down to 10% RH and the values of resistance of the sensing elements recorded with change in % RH. All sensing elements manifest acceptable hysteresis values in the range ±2% to ±5%, which is comparable to the commercial sensors.

Ageing is a significant problem in the sensing devices based on metal oxides. In humidity sensors ageing mechanisms may be due either to prolonged exposure of surface to high humidity, adsorption of contaminants preferentially on the cation sites, loss of surface cations due to vaporization, solubility and diffusion, or annealing to a less reactive structure, migration of cations away from the surface due to thermal diffusion. Generally, more sensitive a material is to humidity more is the effect of aging on sensing elements. After the study of humidity sensing properties, sensing elements were kept in laboratory environment and the characteristics of humidity sensing were regularly monitored. For analysing the effect of ageing, sensing properties of these elements were examined again in the humidity control chamber after six months and variation of resistance with % RH recorded and analyzed. For all the sensing elements annealed at 600°C, values were generally repeatable within ±2% in the 10%−99% RH range after six months. Response/recovery time is defined as the time taken to achieve 90% of the initial total resistance variation during the humidification and desiccation processes. As the annealing temperature increased the response/recovery time decreased. Response and recovery time for the sensing element of 1% MnO_2 doped ZnO for the annealing temperature 600°C were 64 and 162 seconds, respectively. The response and recovery time for the sensing element of undoped ZnO annealed at 600°C were 89 and 312 seconds, respectively.

IV. CONCLUSIONS

X-ray diffraction study confirmed the presence of zinc oxide and its minimum average crystallite size was 47.5 nm. The doping of MnO_2 enhanced crystallization and decreases the crystallite size. The minimum average crystallite size was 31.7 nm for 1.0 weight% MnO_2 doped zinc oxide. With increase in the concentration of MnO_2 the pores increased. The optical band gap of the undoped zinc oxide was found to be 4.05 eV. The value of band gap decreased with increase in the MnO_2 doping concentration. The sensitivity increased with increase in annealing temperature. The sensitivity for the pure sample of ZnO increased from 2100 KΩ/%RH to 3400 KΩ/%RH when the annealing temperature was increased from 300 to 600 ℃. For 1.0% MnO_2 in ZnO the sensitivity increased from 10410 KΩ/%RH to 13610 KΩ/%RH when the annealing temperature was increased from 300 to 600 ℃. The sensitivity increased with increase in doping % of MnO_2 in ZnO. The sensitivity of undoped ZnO for the annealing temperature 600℃ was 3400 KΩ/%RH whereas the sensitivity of the 1.0% MnO_2 doped ZnO was 13610 KΩ/%RH for the same annealing temperature 600℃. The hysteresis was within ±2 to ±5% and aging within ±2%. Response and recovery time for the sensing element of 1% MnO_2 doped ZnO for the annealing temperature 600°C were 64 and 162 seconds, respectively.

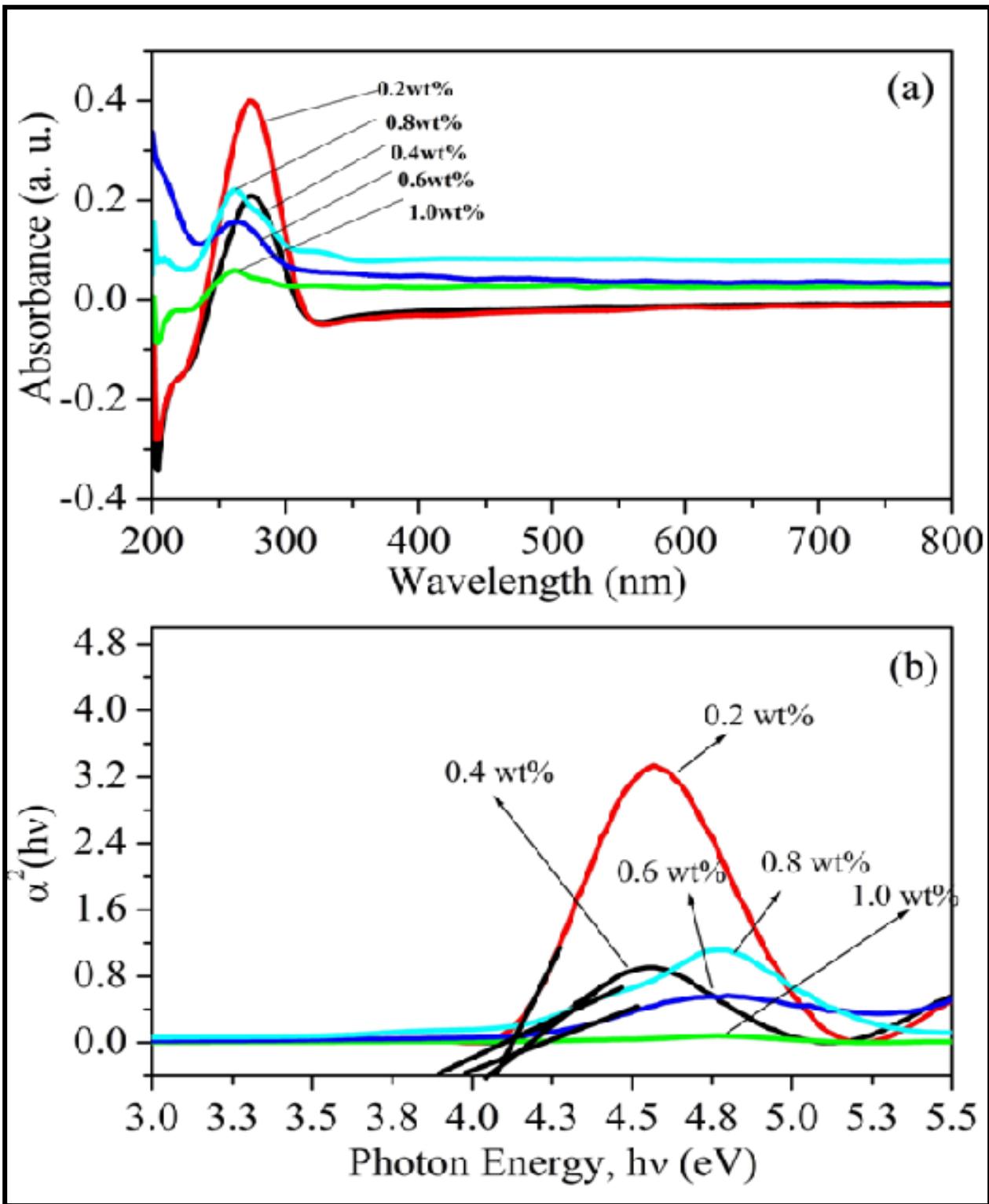**Figure 1.** UV-Visible spectroscopy of ZnO-MnO$_2$ in the wave number 200-800 annealed at 600˚C (a) for sensing elements Z$_1$, Z$_2$, Z$_3$, Z$_4$, Z$_5$ and Z$_6$. (b) Tauc plots of α^2 (hυ) versus photon energy (hυ) for sensing elements Z$_1$, Z$_2$, Z$_3$, Z$_4$, Z$_5$ and Z$_6$.
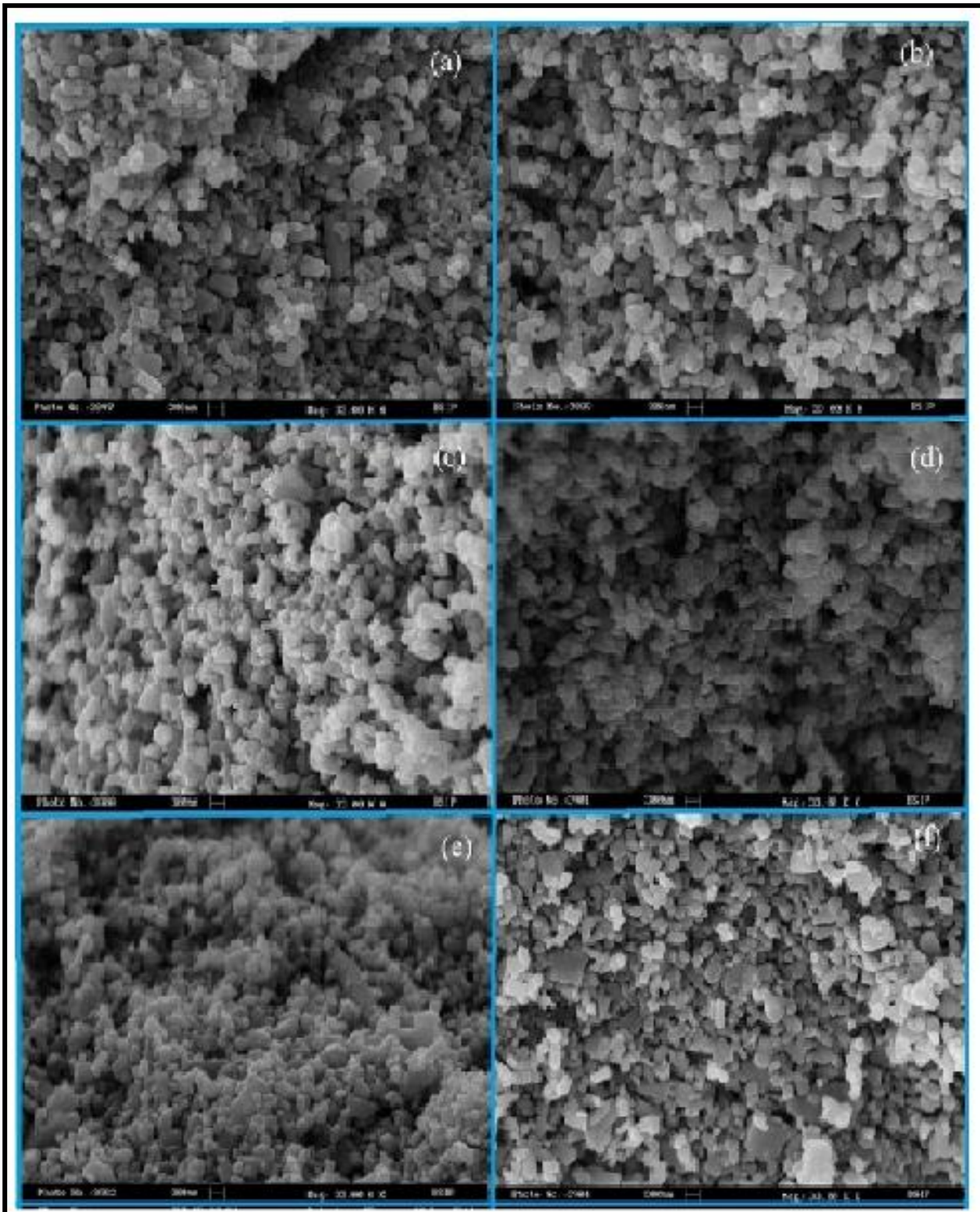
Figure 2. Surface microstructure of ZnO and ZnO-MnO$_2$ composite at 600°C, (a) Pure ZnO, (b) ZnO-0.2 weight % MnO$_2$ and (c) ZnO-0.4 weight % MnO$_2$ (d) ZnO-0.6 weight % MnO$_2$ (e) ZnO-0.8 weight % MnO$_2$ and (f) ZnO-1.0 weight % MnO$_2$.
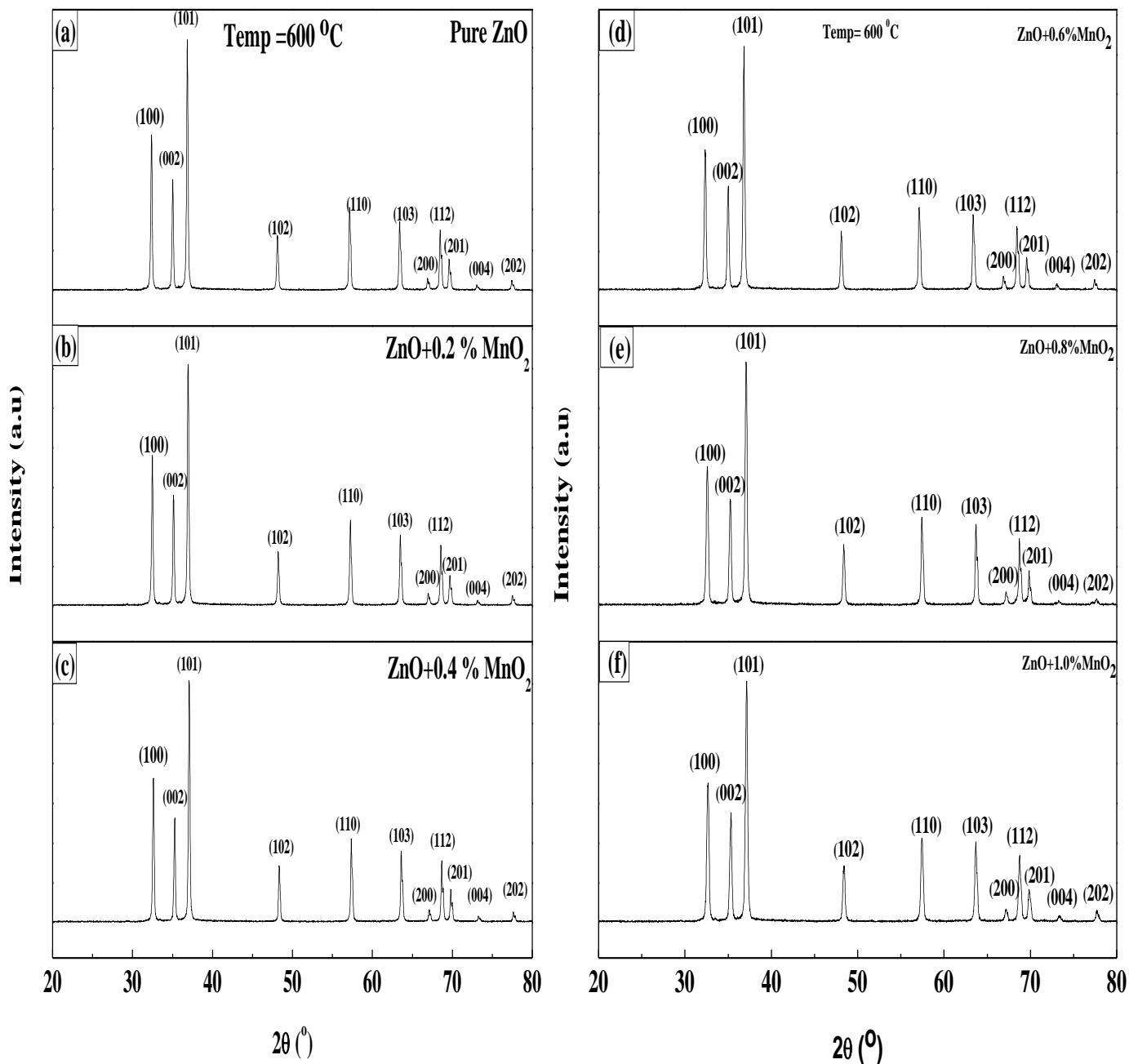
Figure 3. XRD Pattern of ZnO and ZnO-MnO$_2$ Composite in scanning range 20°-80° annealed at 600^oC, (a) Pure ZnO, (b) ZnO-0.2 weight % MnO$_2$ and (c) ZnO-0.4 weight % MnO$_2$. (d) ZnO-0.6 weight % MnO$_2$ and, (e) ZnO-0.8 weight % MnO$_2$ and (f) ZnO-1.0 weight % MnO$_2$.
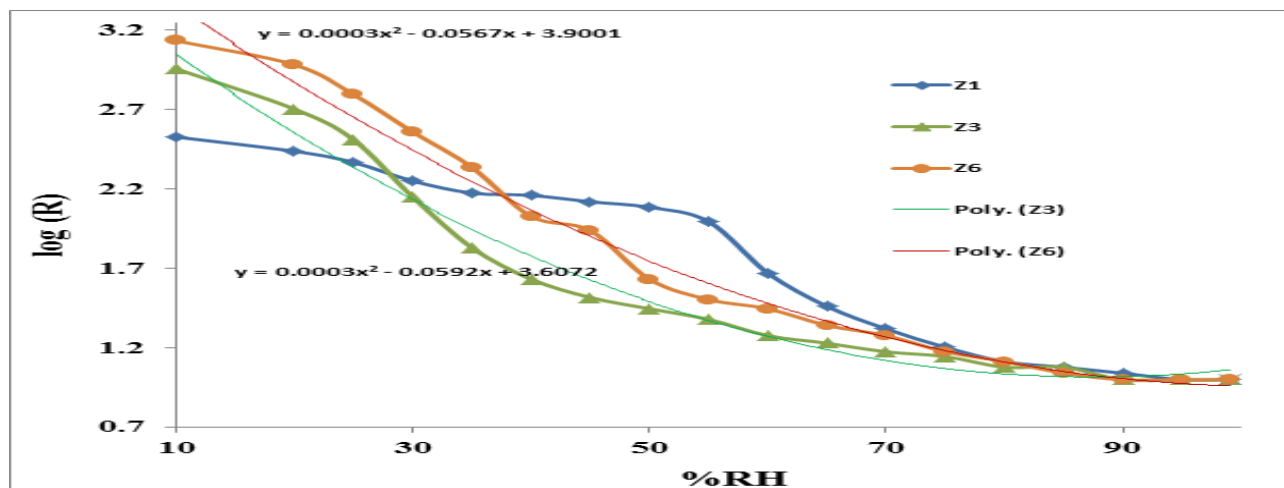
Figure 4. Logarithmic Plot of resistance values versus variation of % RH for sensing elements Z_1, Z_3, and Z_6.
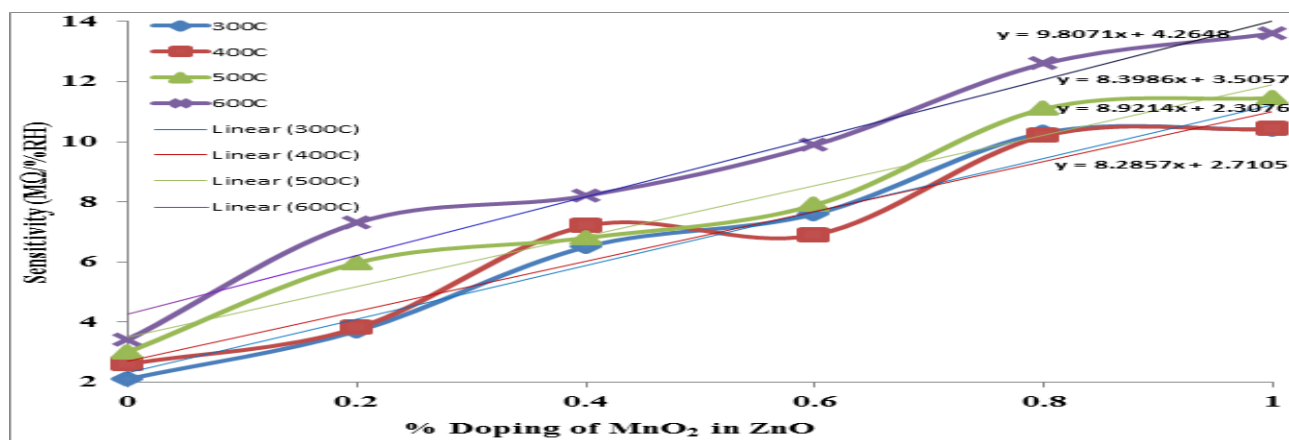

Figure 5. Change in sensitivity with change in annealing temperature and % doping of MnO_2 in ZnO.

REFERENCES

[1] Z. M. Rittersma, "Humidity sensor", Encycl. Sens., Vol.4, pp. 481–509, 2006.

[2] S. Muto, O. Suzuki, O. Amano, M. Morisawa, "A plastic optical fibre sensor for real-time humidity monitoring", Meas.Sci. Technol.,Vol.14, pp. 740–746, 2003.

[3] N. K. Pandey, K. Tiwari, A. Roy, A. Mishra, A. Govindan. "Ag-Loaded WO_3 Ceramic Nanomaterials: Characterization and Moisture Sensing Studies", International Journal of Applied Ceramic Technology, Vol.10, Issue.1, pp. 150-159, 2013.

[4] B. C. Yadav, N. K. Pandey, A. K. Srivastava, P. Sharma, "Optical humidity sensors based on titania Films fabricated by sol-gel and thermal evaporation", Journal of Measurement Science and Technology, Vol.18, No.1, pp. 260-264, 2007.

[5] X. S. Niu, W. P. Du, W. M. Du, "Preparation and gas sensing properties of ZnM_2O_4 (M = Fe, Co, Cr)", Sensors and Actuators B, Vol.99, Issue. 2-3, pp. 405-415, 2004.

[6] Y. M. Zhang, Y. T. Lin, J. L. Chen, J. Zhang, Z. Q. Zhu, Q. J. Liu, "A high sensitivity gas sensor for formaldehyde based on silver doped lanthanum ferrite", Sensors and Actuators B, Vol. 190, pp.171– 176, 2014.

[7] B. Levasseur, S. Kaliaguine, "Methanol oxidation on $LaBO_3$ (B = Co, Mn, Fe) perovskite-type catalysts prepared by reactive grinding", Applied Catalysis A, Vol.343, Issue. 1-2, pp. 29–38, 2008.

[8] J. W. Yoon, M. L. Grilli, E. D. Bartolomeo, R. Polini, E. Traversa, "The NO_2 response of solid electrolyte sensors made using nano-sized $LaFeO_3$ electrodes", Sens. Actuators B, Vol.76, Issue. 1-3, pp. 483–488, 2001.

[9] T. Ishihara, M. Ando, M. Enoki, Y. Takita, "Oxide ion conductivity in $La(Sr)Ga(Fe,Mg)O_3$ and its application for solid oxide fuel cells", Journal of Alloys and Compounds, Vol.408, pp. 507–511, 2006.

[10] X. J. Zhang, H. B. Liang, F. X. Gan, "Novel anion exchange method for exact antimony doping control of stannic oxide nanocrystal powder", Journal of America Chemistry Society, Vol.89, Issue. 3, pp. 792−798, 2006.

[11] Y. Guo, J. Wang, R. Huang, "Electrical and optical properties transparent and conductive Sb-doped SnO_2 films", Journal of Inorganic Materials, Vol.17, pp. 131−138, 2002.

[12] B. K. Meyer, "Bound exciton and donor–acceptor pair recombinations in ZnO", Physica Status Solidi B, Vol.241, Issue. 2, pp. 241-231, 2004.

[13] O(Ed.). Madelung, "Semiconductors "Group IV Elements and III—V Compounds)", Data in science and technology. Springer-Verlag Berlin, ISBN 3-540-53150-5, 164 Seiten, brosch., Preis.; Vol.78, 1991.

[14] Y. Chen, D. Bagnall, T. Yao, "ZnO as a novel photonic material for the UV region", Mater. Sci. Eng. B, Vol.75, Issue. 2-3, pp. 190, 2000.

[15] N. J. Dayan, S. R. Sainkar, R. N. Karekar, R. C. Aiyer, "Formulation and characterization of ZnO:Sb thick-film gas sensors", Thin Solid Films,Vol.325, Issue. 1-2, pp. 325-254, 1998.

[16] N. Saito, H. Haneda, T. Sekiguchi, N. Ohashi, L. Sakaguchi, K. Koumoto, "Low-temperature fabrication of light-emitting ZnO micropatterns using self-assembled monolayers", Adv. Mater, Vol.14, Issue. 6, pp. 418, 2002.

[17] K. L. Chopra, S. R. Das, "Thin Film Solar Cells" (New York: Plenum), Vol.12, Issue. 2-3, pp. 321, 1983.

[18] S. Salam, M. Islam, M. Alam, A. Akram, M. Ikram, A. Mahmood, M. Khan, M. Mujahid, "The effect of processing conditions on the structural morphology and physical properties of ZnO and CdS thin films produced via sol–gel synthesis and chemical bath deposition techniques", Adv. Nature Sci. Nanosci. Nanotechnol., Vol.2, pp. 045001, 2011.

[19] N. T. Hung, N. D. Quang, S. Bernik, "Electrical and microstructural characteristics of ZnO–Bi2O3-based varistors doped with rare-earth oxides", Mater. Res., Vol.16, Issue. 10, pp. 2817, 2001.

[20] D. T. Chieng, P. D. Long, N. H. Lam, P. V. Hoi, "Synthesis, characterization and properties of Mn-doped ZnO nanocrystals", Adv. Nature Sci.: Nanosci. Nanotechnol., Vol.3, No. 3, pp. 035005, 2012.

[21] L. F. Dong, L. Z. Cui, Z. K. Zhang, "Gas sensing properties of nano-ZnO prepared by arc plasma method", Nanostruct. Mater., Vol.8, pp. 815, 1997.

[22] J. J. Wu, S. C. Liu, " Low-temperature growth of well-aligned ZnO nanorods by chemical vapor deposition", Adv. Mater., Vol.14, Issue. 3, pp. 215, 2002.

[23] P. D. Yang, H. Q. Yan, S. Mao, R. Russo, J. Johnso, R. Saykally, "Controlled growth of ZnO nanowires and their optical properties", Adv. Funct. Mater., Vol.12, Issue. 5, pp. 323, 2002.

[24] Y. C. Kong, D. P. Yu, B. Zhang, W. Fang, S. Q. Feng, "Ultraviolet- emitting ZnO nanowires synthesized by a physical deposition approach", Appl. Phys. Lett., Vol.78, pp. 407, 2001.

[25] Y. Dai, Y. Zhang, Q. K. Li, C. W. Nan, "Synthesis and optical properties of tetrapod-like zinc oxide nanorods", Chem. Phys. Lett., Vol.83, pp.358, 2002.

[26] C. Bauer, G. Boschloo, E. Mukhtar, A. Hagfeldt, "Electron injection and recombination in Ru(dcbpy)2(NCS)2 Sensitized Nanostructured ZnO", J. Phys. Chem. B., Vol.105 (24), pp. 5585-5588, 2001.

[27] J. Zhou, N. S. Xu, Z. L. Wang, "Dissolving behavior and stability of ZnO wires in biofluids:A study on biodegradability and biocompatibility of ZnO nanostructures", Adv. Mater., Vol.18, Issue. 18, pp. 2432, 2006.

[28] C. L. Zhu, Y. J. Chen, R. X. Wang, L. J. Wang, M.S. Cao, X. L. Shi, "Synthesis, multi-nonlinear dielectric resonance, and excellent electromagnetic absorption characteristics of Fe3O4/ZnO core/shell nanorods", Sensors and Actuators B, Vol.140, Issue. 1, pp. 185, 2009.

[29] N. K. Pandey, K. Tiwari, A. Roy, "Cu2O doped ZnO as mosture sensor", Christ Church New Zealand, pp. 5387, 2009.

[30] X. Zhou, J. Zhang, T. Jiang, X. Wang, Z. Zhu, "Humidity detection by nanostructured ZnO: a wireless quartz crystal microbalance investigation", Sens. Actuators A, Vol.135, Issue.1, pp. 209–214, 2007.

[31] Y. Qiu, S. Yand, "ZnO nanotetrapods: controlled vapour-phase synthesis and application for humidity sensing", Adv. Funct. Mater., Vol.17, Issue. 8, pp. 1345–1352, 2007.

[32] S. Dixit, A. Srivastava, R. K. Shukla, "ZnO thick film based opto-electronic humidity sensor for wide range of humidity", Opt. Rev.,Vol.14, Issue. 4, pp. 186–188, 2007.

[33] J. Xu, Y. Chen, D. Chen, J. Shen, "Hydrothermal synthesis and gas sensing characters of ZnO nanorods", Sens. Actuators B, Vol.113, Issue. 1, pp. 526–531, 2006.

[34] C. S. Rout, S. H. Krishna, S. R. C. Vivekchand, A. Govindaraj, C. N. R. Rao, "Hydrogen and ethanol sensors based on ZnO nanorods, nanowires and nanotubes", Chem. Phys. Lett., Vol. 418, Issue. 4-6, pp. 586–590, 2006.

[35] S. Roy, S. Basu, "Improved zinc oxide film for gas sensor application", Bull. Mater. Sci., Vol.25, Issue. 6, pp. 513–515, 2002.

[36] F. Xu, K. Yu, G. Li, Q. Li, Z. Zhu, "Synthesis and field emission of four kinds of ZnO nano structure: nanosleeve-fishes, radial nanowire arrays, nanocombs and nanoflowers", Nanotechnology, Vol.17, No.12, pp. 2855–2859, 2006.

[37] C. Xu, M. Kim, J. Chun, D. E. Kim, "The selectively manipulated growth of crystalline ZnO nanostructures", Nanotechnology, Vol.16, No.10, pp. 2104–2110, 2005.

[38] V. Jeseentharani, B. Jeyaraj, J. Pragasam, A. DaySnan, K. S. Nagaraja, "Humidity sensing properties of CuO, ZnO and NiO composites", Sens. Transducers J., Vol.113, Issue. 2, pp. 48, 2010.

[39] T. R. N. Kutty, N. Raghu, "Electrical conductivity of Cu-doped ZnO and its change with hydrogen implantation", Appli.Phys. Lett., Vol.54, No.18, pp. 1796, 1989.

[40] S. P. Yawale, S. S. Yawale, G. T. Lamdhade, "Tin oxide and zinc oxide based doped humidity sensors", Sens. Actuators A, Vol.135, Issue. 2, pp. 388, 2007.

[41] Y. Li, M.J. Yang, Y. She, "Humidity sensors using in-situ synthesized sodium polystrenesulfonate/ZnO nanocomposites", Talanta, Vol.62, Issue. 4, pp. 707, 2004.

[42] M. Matsuguchi, Y. Sadaoka, Y. Sakai, T. Kuroiwa, A. Ito, "A capacitive-type humidity sensor using cross-linked poly (methyl-methacrylate) thin films", J. Electrochem. Soc., Vol.138, Issue. 6, pp. 1862-1865, 1991.

[43] Y. Y. Qui, C. Azeredo-Leme, L. R. Alcacer, J. E. Franca, "A cmos humidity sensor with on-chip calibration", Sens. Actuators A, Phys., Vol.92, Issue. 1–3, pp. 80, 2001.

[44] M. Dokmeci, K. Najafi, "A high-sensitivity polyimide capacitive relative humidity sensor for monitoring anodically bonded hermetic micropackages", J. Microelectromech. Syst., Vol.10, Issue. 2, pp. 197, 2001.

[45] M. Matsuguchi, Y. Sadaoka, Y. Sakai, T. Kuroiwa, A. Ito, "A capacitive-type humidity sensor using cross-linked poly (methyl-methacrylate) thin films", J. Electrochem. Soc., Vol.138, Issue. 6, pp. 1862-1865, 1991.

[46] P. Pascariu, A. Airinei, N. Olaru, I. Petrila, V. Nica, L. Sacarescu, F. Tudorache, "Microstructure, electrical and humidity sensor properties of electrospun, NiO–SnO2 nanofibers", Sens. Actuators B, Vol.222, pp. 1024-1031, 2016.

[47] M. Zhuo, Y. Chen, J. Suna, H. Zhang, D. Guo, H. Zhang, "Humidity sensing properties of a single Sb doped SnO2 nanowire field effect transistor", Sens. Actuators B, Vol.186, pp.78-83, 2013.

[48] Y. Zhou, J.D. Grunwaldt, F. Krumeich, K. B. Zheng, G. R. Chen, J. Stotzel, "Hydrothermal synthesis of Bi6S2O15 nanowires: structural, in situ EXAFS, and humidity-sensing studies", Small., Vol.6, Issue. 11, pp. 1173-1179, 2010.

[49] D. Toloman, A. Popa, M. Stan, C. Socaci, A. Biris, G. Katona, "Reduced graphene oxide decorated with Fe doped SnO2 nanoparticles for humidity sensor", Appl. Surf. Sci., Vol.402, pp. 410-417, 2017.

[50] M. Parthibavarman, V. Hariharan, C. Sekar, "High-sensitivity humidity sensor based on SnO2 nanoparticles synthesized by microwave irradiation method", Mater. Sci. Eng., Vol.31, Issue. 5, pp. 840-844, 2011.

[51] D. Zhang, X. Zong, P. Li, Z. Wu, Y. Zhang, "Ultrahigh-performance impedance humidity sensor based on layer-by-layer self-assembled Tin disulfide/Titanium dioxide nanohybrid film", Sens& Act. B Chemical, Vol.226, pp. 52-62, 2018.

[52] N. K. Pandey, K. Tiwari, A. Roy, "Ag doped nanomaterials as relative humidity sensor", IEEE Sensors Journal, Vol.11, No.11, pp. 2911-2918, 2011.

[53] N. K. Pandey, K. Tiwari, A. Roy, "Moisture sensing application of Cu2O doped ZnO nanocomposites", IEEE Sensors Journal, Vol.11, No.9, pp. 2142-2148, 2011.

[54] N. K. Pandey, A. Roy, A. Kumar, "Characterization of WO3-SnO2 nanocomposites and application in humidity sensing", Sensors & Transducers , Vol.125, No.2, pp. 89, 2011.

[55] J. J. Wu, S. C. Liu, " Low-temperature growth of w ell-aligned ZnO nanorods by chemical vapor deposition", Adv. Mater., Vol.14, Issue. 3, pp. 215, 2002

[56] R. K. Sharma, S. Patel, K. C. Pargaien, "Synthesis, characterization and properties of Mn-doped ZnO nanocrystals", Adv. Nat. Sci., Nanosci. Nanotechnol., Vol.3, pp. 1-5, 2012.

[57] K. S. Chou, T. K. Lee, F. J. Liu, "Sensing mechanism of porous ceramic as humidity sensor", Sensors Actuators B, Vol.56, Issue. 1-2, pp. 106-111, 1999.

[58] J. Zhao, A. Bulduml, J. Han, J. P. Lu, "Fast humidity sensors based on CeO2 nanowires", Nanotechnology, pp. 13195, 2002.

[59] Z. Chen, C. Lu, "Humidity sensor: a review of material and mechanisms", Sensor Lett., Vol. 3, No.4, pp. 274-295, 2005.

[60] J. H. Anderson, G. A. Parks, "Theoretical relations among rate constants, barriers and broensted slopes of chemical reactions", J. Phys. Chem., Vol.72, No.3, pp. 891–899, 1968.

[61] W. M. Sears, "Hydrothermal synthesis of nitrogen and boron co-doped carbon quantum dots for application in acetone and dopamine *sensor* and multicolor cellular imaging", Sensors Actuators B, Vol.281, pp. 34-43, 2018.

[62] X. Q. Fu, C. Wang, H. C. Yu, Y. G. Wang, T. H. Wang, "Synthesis and gas sensing properties of α-Fe2O3@ZnO core–shell nanospindles", Nanotechnology, Vol.22, No.18, pp. 185501, 2011.

[63] C.H. Hu, C.H. Xia, F. Wang, M. Zhou, P. F. Yin, X.Y. Han, "Synthesis of Mn doped CeO2 nanorods and their application as humidity sensor", Bull. Mater. Sci., Vol.34, Issue. 5 pp.1033-1037, 2011.

AUTHORS PROFILE

Profesor Narendra Kumar Pandey graduate with Honors in physics from St. Xavier's College,Ranchi,India,in 1985. He finished his Post Graduation and Doctorate degree from the Indian Insitute of Technology, Delhi, in 1995.He is a Profesor with the department of Physics, from University of Lucknow, Lucknow India. His areas of intrest include humidity and gas sensing,nanotechnology,optical fiber sensor, fiber Bragg grating etc.
Email- nkp1371965@gmail.com

Mr.Vikas Kumar Verma perused BSc degree in 2009 & M.Sc.(Physics) in 2011 from University of Lucknow, Lucknow India. He is working as research scholar and their work is **"Synthesis, Characterization and Humidity Sensing Application(s) of Undoped and Transition Metal Doped ZnO"**.
Email- vikasverma37@gmail.com